TISSUE ENGINEERING: Part C
Volume 15, Number 2, 2009

DOI: 10.1089/ten.tec.2008.0343

Quadrupole Magnetic Sorting of Porcine Islets of Langerhans

Rustin M. Shenkman, Ph.D.,[1] Jeffrey J. Chalmers, Ph.D.,[1] Bernhard J. Hering, M.D.,[2]
Nicole Kirchhof, D.V.M.,[3] and Klearchos K. Papas, Ph.D.[2]

Islet transplantation is emerging as a treatment option for selected patients with type 1 diabetes. Inconsistent isolation, purification, and recovery of large numbers of high-quality islets remain substantial impediments to progress in the field. Removing islets as soon as they are liberated from the pancreas during digestion and circumventing the need for density gradient purification is likely to result in substantially increased viable islet yields by minimizing exposure to proteolytic enzymes, reactive oxygen intermediates, and mechanical stress associated with centrifugation. This study capitalized on the hypervascularity of islets compared with acinar tissue to explore their preferential enrichment with magnetic beads to enable immediate separation in a magnetic field utilizing a quadrupole magnetic sorting. The results demonstrate that (1) preferential enrichment of porcine islets is achievable, but homogeneous bead distribution within the pancreas is difficult to achieve with current protocols; (2) greater than 70% of islets in the dissociated pancreatic tissue were recovered by quadrupole magnetic sorting, but their purity was low; and (3) infused islets purified by density gradients and subsequently passed through quadrupole magnetic sorting had similar potency as uninfused islets. These results demonstrate proof of concept and define the steps for implementation of this technology in pig and human islet isolation.

Introduction

Islet transplantation is emerging as a treatment option for selected patients in whom type 1 diabetes is complicated by frequent acute or progressing chronic complications.[1–7] Inconsistent isolation, purification, and recovery of large numbers of high-quality islets remain substantial impediments to progress in the field.

Current human islet purification protocols rely on the density differential between islets and exocrine and ductal pancreatic tissue. However, density gradients may have undesirable effects on cells such as exposure to potentially toxic chemicals, prolonged exposure to proteolytic enzymes, reactive oxygen intermediates, and mechanical stress associated with centrifugation.[8–12]

Removing islets as soon as they are liberated from the pancreatic tissue mass during isolation and circumventing the need for density gradient purification can potentially result in substantially increased viable islet yields. Instantaneous separation of liberated islets would minimize exposure to proteolytic enzymes, reactive oxygen intermediates, mechanical stress associated with centrifugation, and ischemic stress associated with extended processing. Magnetic separations are attractive because they offer the potential of high throughput and high selectivity. The versatility, availability, and relatively low cost of permanent magnets with powerful magnetic fields have facilitated their recent application in biological separations.[9,12,13]

Magnetic cell isolation by infusion of magnetic beads into the vasculature was first applied to the isolation of renal glomeruli. Iron oxide infused into murine left ventricular cavities became physically trapped within the glomeruli, which were collected with a bar magnet after tissue disruption.[14] This technique was extended by perfusing magnetite (Fe_3O_4) into the murine aorta. The magnetite particles were preferentially trapped within the capillaries of the renal glomeruli. After mechanically dispersing the kidney tissue, a bar magnet was paired with a Dynal MPC™-6 magnetic particle concentrator (MPC). The authors recovered 28% of total renal glomeruli at 90% purity.[15,16]

It had been observed that pancreatic islets and renal glomeruli have similar angioarchitectures.[9] Pinkse *et al*. (2004) injected suspensions of magnetite particles into the descending rat aorta that were subsequently trapped within the narrow islet microcapillaries,[9] and after digestion a Dynal® MPC separation system was used to isolate islets. Magnetic separation yielded significantly more islets per pancreas than was obtained using conventional density gradient isolation. In addition, the authors reported that the magnetic separation technique was three times faster than the conventional

[1]Department of Chemical and Biomolecular Engineering, The Ohio State University, Columbus, Ohio.
[2]Diabetes Institute for Immunology and Transplantation, University of Minnesota, Minneapolis, Minnesota.
[3]Medtronic, Inc., Minneapolis, Minnesota.

isolation method, which contributed to a significantly higher viability in culture of the magnetically purified islets. Further, density gradient-separated islets lost their β-cells and α-cells over time, suggesting that the islets were harmed by chemical and/or mechanical stress. Transplantation of magnetically separated islets into diabetic rats restored euglycemia for over 2 months, and the Fe_3O_4 did not cause an inflammatory response in rat kidney capsules.[9] More recently, Töns *et al*. (2008) reported infusing this same Fe_3O_4 solution into 10 human research pancreata.[17] The authors reported that 60% to 80% of recovered islets contained magnetite aggregates compared to only 0.4% to 2.8% in the exocrine tissue. The Fe_3O_4 did not otherwise affect the digestion protocol; however, the recovered islets were usually only 30% to 40% pure.[17]

Given the limitations of current density gradient purification protocols, the initial success reported above with the use of magnetic technology in rat islet separation, and the limitations noted when applying this technology to human islet processing, the application of a recently developed high-throughput, high-gradient, continuous quadrupole magnetic sorting (QMS) technology[18,19] for use in porcine islet isolation was explored.

Materials and Methods

Pancreas labeling and islet isolations

All animal procedures were approved by the Institutional Animal Care and Use Committee (IACUC) and performed by the Islet Processing Core at the Diabetes Institute for Immunology and Transplantation at the University of Minnesota. Pancreata from ~600 lb Landrace sows were clamped and divided into splenic, connecting, and duodenal lobes. The portal vein and hepatic and splenic arteries were clamped and tied *in situ*. The celiac trunk of the aorta was catheterized, and 400 mL PBS solution containing 4×10^9 Dynabeads® was injected. Neutral Red dye in the PBS solution gave a visual indication of the progression of the bead solution into the three lobes. These infused organs were subsequently processed for histological evaluation or they were digested for islet isolation using the Ricordi method.[20]

To compare infused versus uninfused islets obtained from the same pancreas, the splenic pancreatic lobe alone was infused with magnetic beads. This allowed infused and uninfused lobes from the same pancreas to be independently processed for islet isolation. Both infused and uninfused dissociated pancreatic tissues were processed for density gradient islet purification.[21,22] Density gradient–purified islets from infused lobes were also passed through the QMS system and were compared to those that had not been exposed to QMS. Attempts were also made for purification of islets from pancreatic lobes infused with magnetic beads by passing the unpurified dissociated tissue through QMS without prior density gradient purification. Islets isolated and purified from infused and uninfused lobes were then compared to assess any effects of magnetic label incorporation on islet quality.

QMS system

As described on several occasions,[18,19,23] QMS is a high-throughput, high-gradient, continuous magnetic cell separation system. It was designed for the positive separation of immunomagnetically labeled single cells from a previously labeled cell population. Figure 1 describes the basic QMS mechanism for sorting magnetic from nonmagnetic cell populations. Unlike other systems, the QMS can be operated continuously whereby a cell population containing labeled cells (tissue feed and carrier fluid, stream $\boldsymbol{a}'$ in Fig. 1) and a pure fluid substream (carrier fluid, stream $\boldsymbol{b}'$) are introduced into the separator; unlabeled cells exit in one stream (carrier fluid plus unlabeled cells, stream $\boldsymbol{a}$) and labeled cells in the other (carrier fluid plus magnetically labeled cells, stream $\boldsymbol{b}$).

Magnetic theory

The QMS system has been extensively modeled and tested.[23–27] The ability of immunomagnetically labeled cells to be collected in the magnetic exit stream $\boldsymbol{b}$ (Fig. 1) and the unlabeled cells in the nonmagnetic stream $\boldsymbol{a}$ (Fig. 1) is a function of a number of factors, especially the degree to which the cells are immunomagnetically labeled. Particle labeling may be quantified via the magnetophoretic mobility, a parameter proportional to the magnetic field gradient.

The magnetophoretic mobility of an immunomagnetically labeled cell, m, is theoretically represented by the following equation:

$$\boldsymbol{m}=\frac{\boldsymbol{v_m}}{\boldsymbol{S_m}}=\frac{\phi_p\beta\boldsymbol{ABC}}{3\pi\boldsymbol{D_{cell}}\eta}+\boldsymbol{m_{cell}} \quad (1)$$

where v_m is the magnetically induced velocity, S_m is the magnetic energy gradient, ϕ_p is the field interaction parameter, ABC is the antibody binding capacity of the cell, β is the number of magnetic nanoparticles per ABC, D_{cell} is the diameter of the cell, η is the viscosity of the suspending fluid,

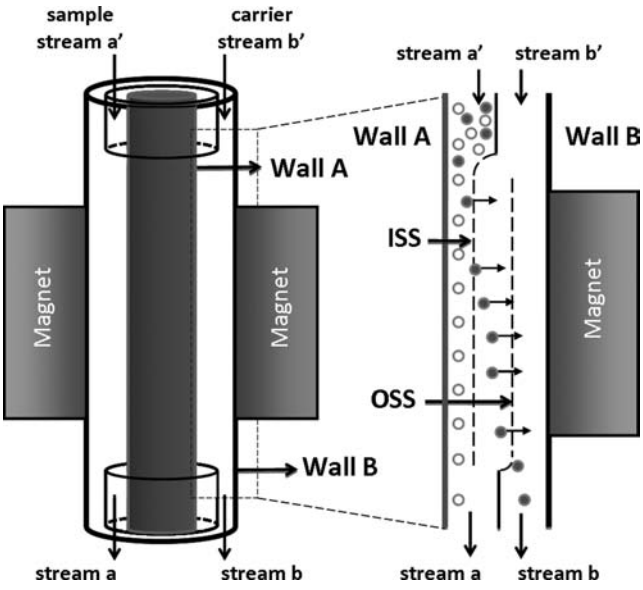

FIG. 1. Schematic depicting the annular QMS channel revealing the inner (ISS) and outer (OSS) split streams. Magnetic cells (or islets) that cross the OSS are continuously sorted. The labeled sample enters as stream a′ along with a carrier stream, b′. The magnetic fraction is collected from stream b.

and m_{cell} is the intrinsic magnetophoretic mobility of the unlabeled cell.[23,28,29] For unlabeled lymphocytes, this mobility has been reported to be -5.2×10^{-5} mm^3 T^{-1} A^{-1} s^{-1}.[28] The field interaction parameter is defined as follows:

$$\phi_p = (\chi_p - \chi_f)V_p \qquad B_0 < B_{sat} \tag{2}$$

or

$$\phi_p = \left(\frac{M_{sat}\mu_0}{B_0} - \chi_f\right)V_p \qquad B_0 \geq B_{sat} \tag{3}$$

where χ_p is the magnetic susceptibility of the magnetic particle, χ_f is the magnetic susceptibility of the suspending buffer, V_p is the volume of the magnetic particle, B_0 is the specific field induction, B_{sat} is the magnitude of the magnetic field induction above which the magnetic particle is saturated, M_{sat} is the moment saturation of the magnetic particle, and μ_0 is the magnetic permeability of free space.[28]

Using an instrument referred to as a cell tracking velocimeter, Zhang *et al*. performed a study characterizing a number of commercial magnetic nanoparticles with respect to the particle size and magnetic susceptibility and compared them to literature values of nanometer-sized and micron-sized particles.[28] With such an analysis, estimates of ϕ_p were made, and these values are presented in Table 1.

Islet quality assessment

Oxygen consumption rate measurements. Oxygen consumption rates (OCR) were measured as previously described.[30] Briefly, islets were suspended in Dulbecco's modified Eagle's medium (Mediatech, Herndon, VA) containing 4.5 g/L glucose and 0.6 g/L L-glutamine without serum (to avoid formation of bubbles) and supplemented with 100 U/mL penicillin, 100 μg/mL streptomycin, and 10 mM HEPES. These islet suspensions were then placed in a 200-μL stirred titanium chamber (Micro Oxygen Uptake System, FO/SYSZ-P250; Instech Laboratories, Plymouth Meeting, PA) maintained at 37°C. After the chamber was sealed, the time-dependent oxygen partial pressure (pO_2) within the chamber was recorded with a fluorescence-based oxygen sensor, and the data at high pO_2 were fit to a straight line. The maximal OCR was evaluated from $OCR = V_{ch}\alpha(\Delta pO_2/\Delta t)$, where $\Delta pO_2/\Delta t$ is the slope of the line, V_{ch} is the chamber volume, and $\alpha = 1.27$ nmol mm Hg^{-1} mL^{-1} is the Bunsen solubility coefficient for oxygen in medium.[31]

ATP quantification. The CellTiter-Glo Luminescent Cell Viability Assay kit (Promega, Madison, WI) was used per manufacturer's instructions to measure the ATP content in islet samples. Luminescence readings were taken on a SpectraMax M5 microplate reader (Molecular Devices, Sunnyvale, CA). Each sample was processed and plated in a 96-well white microplate (Corning 3912; Corning, Corning, NY). Serially diluted ATP was used as a standard (Sigma-Aldrich, St. Louis, MO).

DNA quantification. Islet DNA was measured and used to normalize the OCR and ATP values. To measure DNA content, islet samples, either prepurified by density gradient or hand picked from impure digests, were diluted in an aqueous solution of 1 M ammonium hydroxide and 3.4 mM Triton X-100, and sonicated. DNA content was then determined using the Quant-iT PicoGreen dsDNA kit (Molecular Probes, Eugene, OR) per manufacturer's instructions. Fluorescence readings were taken in 96-well black microplates (Corning) on a SpectraMax M5 microplate reader (Molecular Devices).

Insulin assay. A sample (100 μL) of islets was removed from the main pool, and 400 islet equivalents (IEQ) (defined as spheres with a diameter of 150 μm) were added to a 5 mL tube containing 1400 μL of medium plus 2.8 mM glucose. From this, 80 IEQ (300 μL) were placed into a permeable insert of 12 mm in diameter seated in a culture well containing 700 μL medium plus 2.8 mM glucose. After a 30 min equilibration the inserts containing the islets were removed from their respective wells, drained, blotted, and placed into a culture well containing 1300 μL medium plus 2.8 mM glucose. A 300 μL sample of the supernatant was immediately taken for each of the replicates as a basal time 0 sample. After 60 min, the remaining supernatant was collected as a basal time 1 h sample. The islets were then transferred to a culture well containing medium at 28 mM glucose, and an aliquot of the supernatant was immediately taken as a stimulation time 0 sample. After 60 min, the remaining supernatant was collected as a stimulation time 1 h sample. The amount of insulin present in the supernatant samples was measured

Table 1. Comparison of Normalized Magnetization, M_{SAT}/B_0 (Eq. 3), and Field Interaction Parameter, ϕ_P, of Commercial Magnetite Particles Previously Published in Zhang *et al*.[28]

Magnetic bead	*Lot no.*	M_{sat}/B_0 ($\times10^{-5}$ A^2 N^{-1})	*Diameter (nm)*	Φ_p ($\times10^{-25}$ m^3)
SAP-MACS®	5020305031	110 ± 30	116	8.8 ± 2.1
	5020918049	140 ± 40	67	2.3 ± 0.6
BD Imag®	44023	140 ± 30	231	91 ± 20
Captivate®	71A1-1	38 ± 10	136	5.1 ± 1.4
Dynabeads®			4500	9.2×10^6
Easysep®	2L226593	35 ± 12	142	5.4 ± 2.0
	3A17176	5.5 ± 1.8	160	12 ± 4

Manufacturer information for Table 1: From Zhang *et al*.[28] Streptavidin MACS beads: Catalog number 481–01/02, Miltenyi Biotec, Auburn, CA; BD™ Imag streptavidin bead: Catalog number 551308, BD Pharmingen, San Jose, CA; Captivate™ ferrofluid: Catalog number C-21476, Molecular Probes (Eugene, OR); EasySep™ beads: StemCell Technologies, Vancouver, Canada; DynaBeads M-450, tosylactivated: Invitrogen Dynal AS, Oslo, Norway.

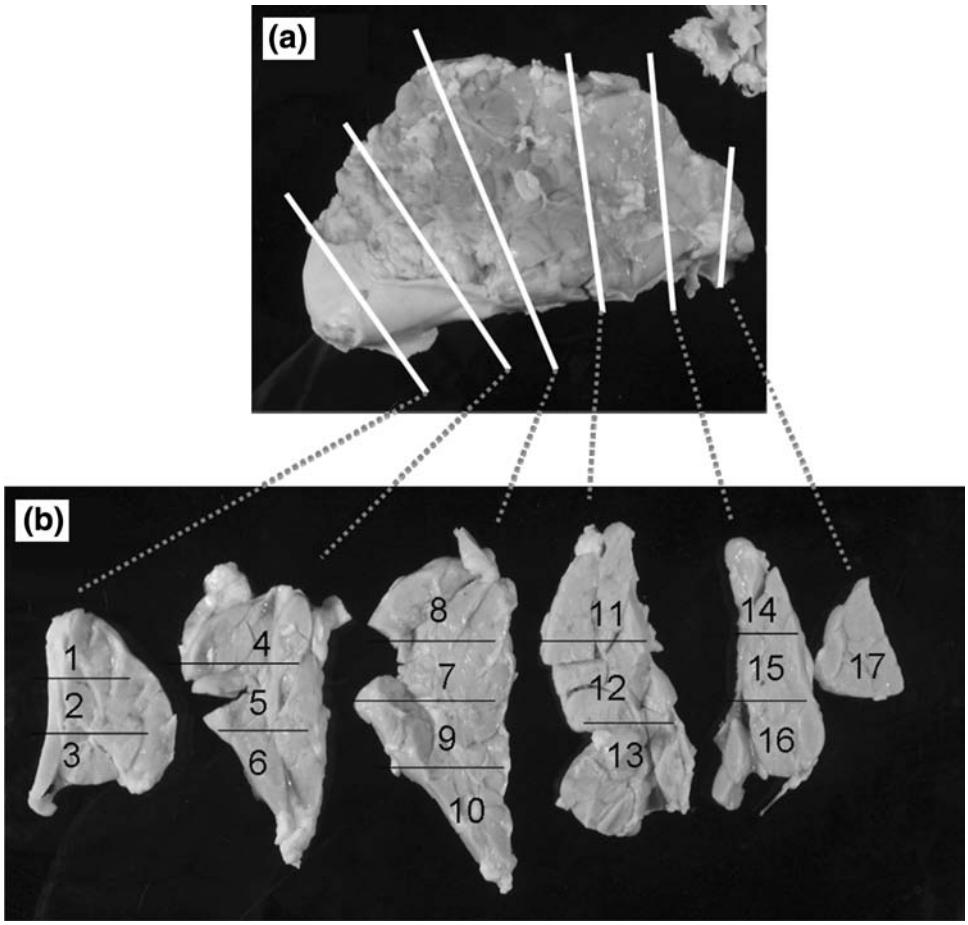

FIG. 2. A porcine pancreas infused as described in the Materials and Methods section was divided into its three lobes (splenic, duodenal, and connecting) and processed for histology. (**a**) The infused splenic lobe was divided into six sections by microtome as indicated by the white lines. (**b**) The six sections depicted in (**a**) were further divided into 17 as indicated by the black lines (sections 1–17). The number of Dynabeads found in each of the examined sections is summarized in Table 2.

using a commercially available insulin ELISA kit (Mercodia, Uppsala, Sweden). The stimulation index is the ratio of the amount of insulin secreted in the presence of high glucose concentration divided by the amount of insulin secreted in the presence of low glucose concentration over the 1 h period. All measurements were conducted in triplicate.

Diabetic nude mouse bioassay. Islet potency *in vivo* was assessed with the diabetic nude mouse bioassay. All animal procedures were approved by the IACUC and performed by the Islet Processing Core at the Diabetes Institute for Immunology and Transplantation at the University of Minnesota. About 2000 IEQ, measured by manual counts on day 2 after isolation, were transplanted under the kidney capsule of nude streptozotocin-induced diabetic (>350 mg/dL blood glucose pretransplant) mice. Diabetes was considered reversed after three consecutive measurements of normoglycemia (<200 mg/dL blood glucose) posttransplant.

Table 2. Visual Dynabead Counts Within the Zones of the Infused Organ Microtome Sections

Location	*Sublocation*	*No. of beads in 20 HPF*	*Frequency of infused islets*	*No. of beads per islet*
A	3	28	Very rare (<5%)	1 to 10
A	6	43	Rare (<10%)	2 to 20
A	7	42	Many (50%)	1 to 20
A	10	>100	Most (75%)	1 to 30
A	12	21	Almost all (85%)	1 to 8
A	14	2	None	0
A	16	3	Very rare (<5%)	1
B	2	0	0	0
B	6	0	0	0
C	3	51 (very uneven)	Often (25%)	1 to 20

Location (column 1) refers to the lobe examined (A, splenic; B, connecting; C, duodenal) and sublocation (column 2) refers to the section of the lobe examined. Lobe sectioning was performed as depicted in Figure 2. Number of beads in the examined region corresponding to 20 high-power fields (HPF) is given in column 3.

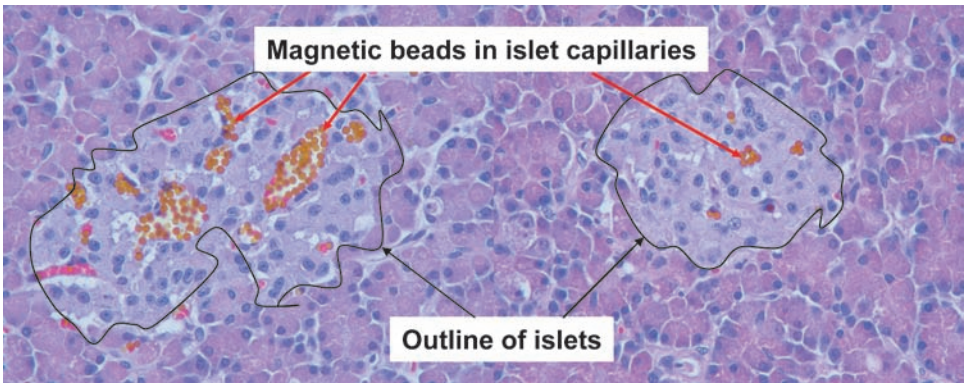

FIG. 3. Micrograph of a pancreatic tissue section infused with magnetic Dynabeads. The periphery of the islets is outlined. Dynabeads (rust colored) are clearly visible within the islets but rare within the surrounding acinar tissue. Colocalization of the magnetic beads within the islets with red blood cells (in pink color) is also evident.

Statistical analysis. All measurements were conducted in at least triplicate, and results are reported as mean ± standard deviation. Statistical comparisons between conditions and runs were performed using the Wilcoxon/Kruskal-Wallis rank test and Tukey Honestly Significantly Different (HSD) least square means test on JMP 6.0.0 (SAS Institute, Cary, NC). The data were approximately normally distributed and unbiased. Results were considered significant for $p < 0.05$.

Results

Tissue labeling and histology of infused porcine pancreas

An example of a porcine pancreas infused with beads and processed for histology is presented in Figure 2. After bead infusion, the pancreas was processed for histology and was divided into splenic, duodenal, and connecting lobes. The lobes were further sectioned for examination under a light microscope. The splenic lobe, which contained the main artery used for bead infusion, was divided into 6 sections and further divided into 17 subsections as shown. The connecting and duodenal lobes were sectioned and labeled in a similar manner.

These slices were examined under the microscope, and the numbers of observable beads were tabulated (Table 2). From this table a virtual bead distribution map was created of the intact three-lobe organ. Dynabeads were found throughout the splenic lobe islets. A narrow cylindrical region of infused Dynabeads extended from the splenic lobe into the duodenal lobe. No Dynabeads were observed in the connecting lobe. It was apparent that the concentration of Dynabeads within the infused pancreas was highest proximal to the infusion point at the splenic lobe. Microscopic observations of the magnetically infused pancreatic tissue indicated that Dynabeads were visible under low magnification in microtome sections of intact pancreatic tissue (Fig. 3) as well as the purified, digested islets (Fig. 4a). The great majority of infused Dynabeads were found within islets rather than exocrine tissue, and it was further observed that in several situations a large number of Dynabeads infused into the splenic lobe never lodged or only very weakly lodged in the tissue. Upon digestion, these beads ended up suspended in the digestion broth. It was observed that when this sample was placed near an appreciable magnetic field such as a Neodymium bar magnet or QMS, the highly magnetic beads formed extended aggregates and chains (Fig. 4b). Particle aggregation is caused by attractions between the dipole moments, μ, of neighboring particles. Dipole moments are induced by an applied magnetic field and are proportional to the magnitude of that field, H:

$$\mu = V_p \cdot \mu_0 \cdot \chi_p \cdot H \tag{4}$$

where V_p is the particle volume, H is the magnitude of the applied field, χ_p is the particle susceptibility, and μ_0 is the permeability of free space. Since the QMS has a much higher field magnitude than a single Neodymium bar magnet, it is a safe assumption that the bead aggregates within the QMS

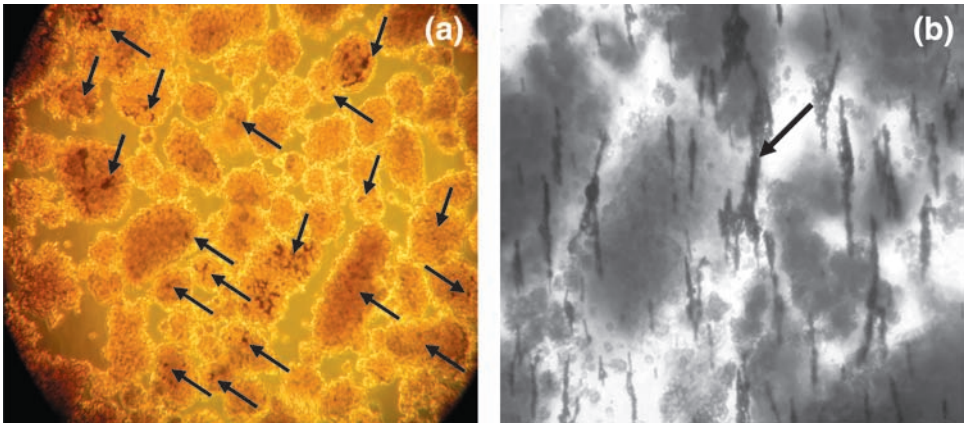

FIG. 4. (**a**) Photograph of density gradient-purified islets. Dynabeads were visible in the majority of purified islets (see arrows). (**b**) Photograph of infused digestate held against a Neodymium bar magnet. Under this strong field, highly magnetic Dynabeads that are not lodged within islets are drawn together to form extended chains (see arrow). It is thought that these "fish nets" carry unlabeled tissue into the magnetic fraction or else pin unlabeled tissue against the QMS channel wall.

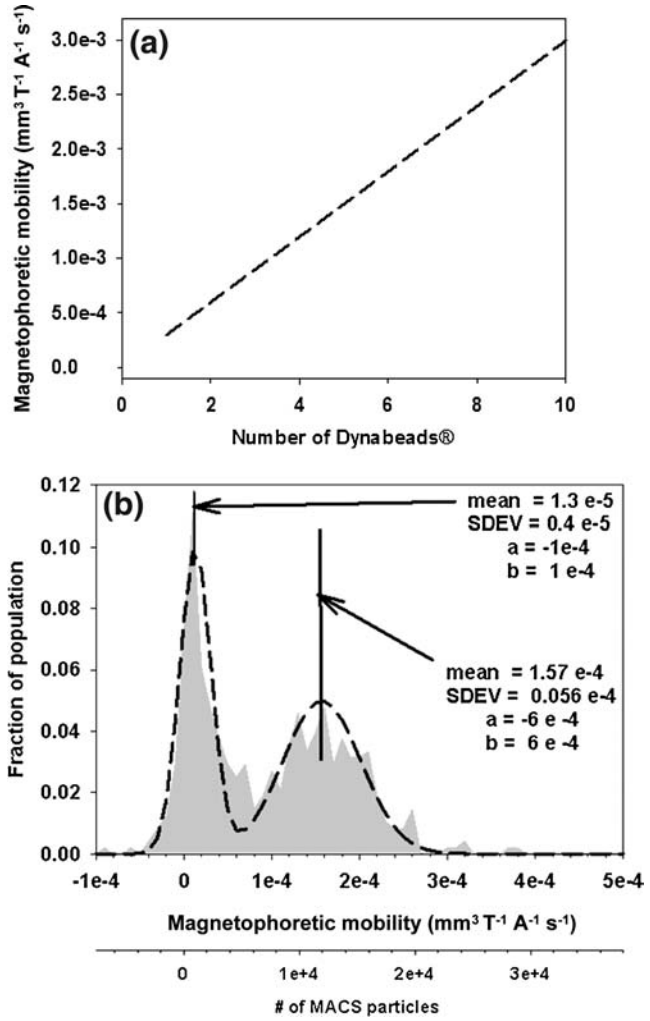

FIG. 5. (**a**) A plot of the theoretical magnetophoretic mobility of a 150 micron sphere as a function of the number of infused Dynabeads. These mobility numbers are quite high when compared to histogram plots of the negative (left histogram) and positive eluents (right histogram) from a immunomagnetic separation of human lymphocytes in a MiniMACS separation system (**b**). The cells were targeted with an anti-CD3 PE label and an anti-PE MACS reagent. Notice that 1.2×10^4 MACS beads impart a single human lymphocyte with the same magnetophoretic mobility that a single 4.5 micron Dynabead gives a 150 micron sphere.

itself would be even more extensive than observable in Figure 4b.

Theoretical mobility and QMS performance

The visual observation that Dynabeads become lodged in the capillaries of islets (Fig. 3) confirmed that infusion of Dynabeads resulted in preferential labeling of islets with magnetic particles. The theoretical magnetophoretic mobility for an IEQ containing between 1 and 1000 Dynabeads was then calculated. Using the Dynabead field interaction parameter ϕ_p from Table 1, a plot of magnetophoretic mobility as a function of the number of infused Dynabeads was devised (Fig. 5a). To put these values of magnetophoretic mobility into perspective, Figure 5b presents a histogram of the

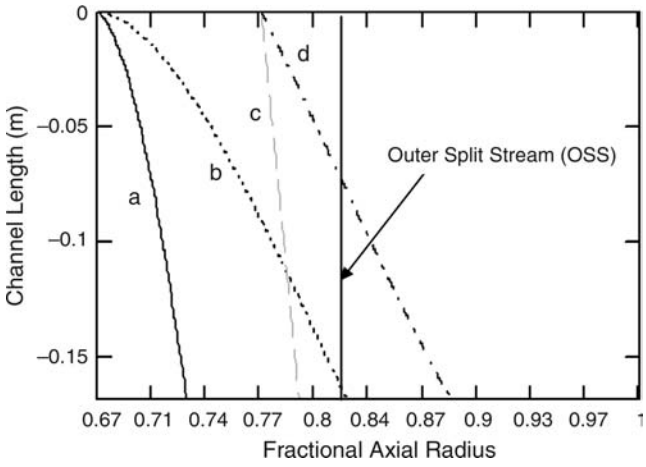

FIG. 6. Modeled trajectories of an IEQ, islet equivalents moving along the QMS channel. The *y*-axis is the channel length and the *x*-axis is the fractional channel radius. Cells may enter near the inner core of the channel (a, b) or near the outer shell of the channel (c, d) with a range of mobilities. An IEQ that crosses the Outer Split Steam leaves with the magnetic fraction.

magnetophoretic mobility of human peripheral blood lymphocytes from Lara and coworkers[32] labeled with an antibody conjugated to a magnetic nanoparticle (MACS® bead). The second *x*-axis gives the theoretical number of MACS particles needed to achieve the given mobility using Equation 1 and the value of the field interaction parameter for a MACS bead determined by Zhang and coworkers.[29] Comparing Figure 5b with 5a, approximately 1.2×10^4 MACS beads impart a single human lymphocyte with the same magnetophoretic mobility that a single 4.5 micron Dynabead gives an IEQ.

The magnetophoretic mobility values determined for a magnetically labeled IEQ were used as previously reported[26] to perform computer simulations of the magnetoviscous force balance within the QMS. From the distribution of the feed cells' magnetophoretic mobility, the outcome trajectory of the IEQ (exit a, exit b in Fig. 1, or deposited on the wall) is given based on the entrance and exit flow rate ratios. Figure 6 shows trajectories of four theoretical IEQ (a, b, c, and d) entering and exiting the QMS channel with respect to the longitudinal and normalized radial coordinates. Particles (in this case IEQ) may enter the channel randomly at any point between the inner (particles a and b) and outer (particles c and d) walls of the feed stream (stream a′ in Fig. 1). For each extreme of the radial starting point, we expect that islets will have a range of magnetophoretic mobilities. Figure 6 presents two values of the IEQ's magnetophoretic mobility for each starting point. The outer split stream represents the radial coordinate that separates the magnetic and nonmagnetic outlet streams (the exit streams b and a in Fig. 1).

In this example, IEQ having the lower mobilities (a and c) will not cross the transport laminar (0.82 on the *x*-axis) regardless of starting position, whereas IEQ having the higher mobility (b and d) will cross split stream and exit in stream b. Model predictions indicate that at a feed stream of 30 mL/min, IEQ will cross the split stream and exit in stream b for a magnetophoretic mobility greater than 3×10^{-4} mm^3 T^{-1} A^{-1} s^{-1}. IEQ with mobility of 5×10^{-4} mm^3 T^{-1} A^{-1} s^{-1}

or greater will impinge the outer wall of the channel and potentially be pinned to that location. From Figure 5a, islets infused with one to five Dynabeads flowing at 30 mL/min should be continuously removed in stream b; IEQ with a greater number of Dynabeads would have to be washed from the channel after removing it from the magnet.

QMS separation of islets

A total of four porcine donor organs were infused and processed for magnetic separation. In the case of the first two donors, P396 and P397, once the pancreata were infused with magnetic beads and digested, the resulting tissue suspensions were split into halves: one half was prepurified by a standard density gradient methodology. Both halves were then fed to the QMS. Two later donors, P411 and P412, were fed to the QMS immediately after digestion without prior purification with density gradients. Manual islet counts via dithizone staining were used to assess the number of islets passing into and out of the QMS. Flow rate, inlet ratio (R_{in}/R_{out}), and feed concentration were varied to test the sensitivity of the recovery. Results of the four studies are given in Table 3.

Quality of Dynabead-infused islets

Studies were also conducted to determine if the presence of Dynabeads within the islets (P382, P383, P396, and P397) and passage through the QMS (P396 and P397) had any deleterious effects on their quality. Figures 7a–c present insulin stimulation index, ATP concentration (μmol mg^{-1} DNA), and OCR per DNA (nmol min^{-1} mg^{-1} DNA), respectively, of uninfused (control) islets and islets infused with Dynabeads. Both sets of islets were purified by density gradient. Islets that were not prepurified with density gradients were highly impure and could not be appropriately tested for quality. Islets purified with density gradients and subsequently passed through QMS were not significantly different in terms of insulin stimulation index, ATP content, or OCR compared to islets from the same batch never subjected to QMS. Although there is significant variability between isolations, the presence of Dynabeads had no statistical effect on islet health (viability and function) as evaluated by these assays.

In addition to the *in vitro* tests, islets were evaluated *in vivo* for their ability to reverse diabetes in mice. About 2000 IEQ from different lobes (with and without infused Dynabeads) of the same donor pancreas were transplanted underneath the kidney capsule of diabetic nude mice as described in the Materials and Methods section. About 75% (3/4) of the mice receiving control islets and 80% (4/5) of mice receiving infused islets regained euglycemia. These data suggest that the presence of magnetic beads within porcine islets does not impair their viability and function as indicated by their ability to reverse diabetes in mice.

Discussion

In this study we attempted to capitalize on the hypervascularity of islets compared with acinar tissue previously reported in the rat[9,33–34] to scale-up and explore the preferential enrichment of porcine islets with magnetic beads, followed by instant purification in a magnetic field utilizing a continuous high-throughput quadrupole magnetic sorter.

It was initially hoped that a simple infusion of a Dynabead suspension into the celiac trunk of the aorta would be sufficient for homogeneous distribution of beads through the porcine pancreas. However, as demonstrated in the Results section, this was not true, and improvements in the bead infusion protocol are clearly needed for homogeneous and consistent islet labeling. The recent detailed characterization of the porcine pancreatic anatomy and the optimization of pancreas procurement and flushing protocols by our group[35] are expected to contribute substantially to the development of techniques for homogeneous bead infusion within the porcine pancreas in the near future. Further, even though Dynabeads were the proper size for the islet microvasculature, they were far more magnetic than necessary for effective QMS with the current system. Use of beads with lower

Table 3. Samples Were Fed to the QMS Immediately After Digestion or After a Prepurification Step by Density Gradients

Donor	*Preparation*	*Flow rate (mL/min)*	R_{in}/R_{out}	*Sample vol. (mL)*	*No. of islets ($\times 10^3$)*	*Islet recovery (%)*
P396	Density Gradient	50	0.2/0.4	30	16	20
	Density Gradient	50	0.2/0.4	30	24	83
	Density Gradient	50	0.2/0.4	30	25	51
	Raw Digest	50	0.2/0.4	30	9	67
P397	Density Gradient	50	0.2/0.4	30	27	70
	Raw Digest	20	0.2/0.4	60	2	66
	Raw Digest	20	0.5/0.5	120	9	39
	Density Gradient	50	0.2/0.4	30	30	39
P411	Raw Digest	30	1.0/0.4	240	3	32
	Raw Digest	10	1.0/0.4	480	10	37
	Raw Digest	50	1.0/0.4	480	33	20
P412	Raw Digest	30	1.0/0.4	175	6	73
	Raw Digest	10	1.0/0.4	175	3	41

R_{in} is the ratio of sample volume (a′) to the total feed volume (a′ + b′), and R_{out} is the ratio of nonmagnetic outlet (a) to the total outlet volume (a + b). Islet recovery refers to the number of islets recovered from the magnetic outlet and rinsed from the channel compared to the number of islets in the feed.

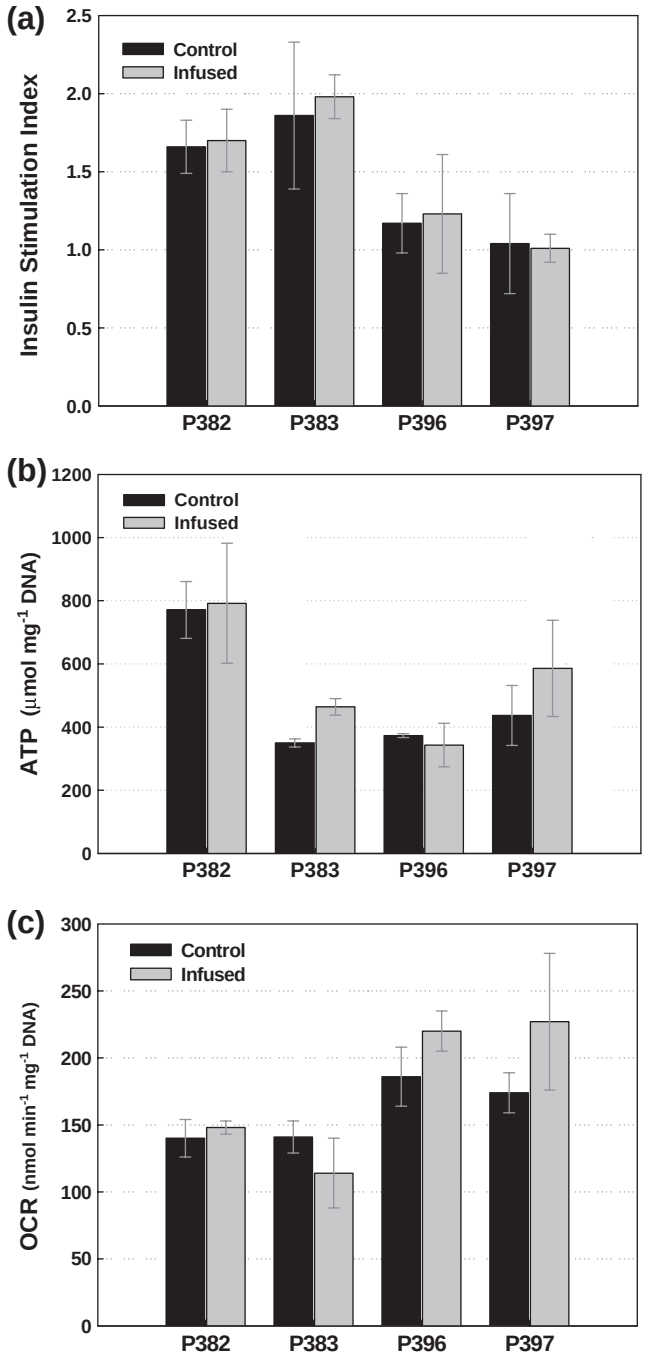

FIG. 7. Stimulation index for glucose-stimulated insulin secretion (**a**), ATP (**b**), and OCR (**c**) measurements from control and infused islets from four separate isolations. Bead infusion did not measurably affect islet viability or insulin secretion as compared to uninfused control islets. OCR, oxygen consumption rates.

magnetic content and/or modified QMS equipment will address this issue.

As the data in Table 3 indicate, when digested islets were first isolated in a density gradient and then a known amount of islets were separated by the QMS, the recovery of the islets ranged from 20% to 83%. When the islets were separated immediately after digestion (referred to as raw digest in Table 3), the recovery from the magnetic separator ranged from 20% to 73%. Since in neither approach was the fraction of islets that contained Dynabeads determined, it is highly likely that the large range of variability of recovery of islets from the QMS system was a function of whether Dynabeads were in the islets, and not whether the islets were preisolated in a density separation step. This is encouraging, since the long-term goal of this work is to replace the density separation with magnetic separation. A further encouraging result was the observation that both the infusion the Dynabeads into the islets and the QMS separation had no apparent physiological effect on the islets as determined by glucose-stimulated insulin secretion, ATP content, OCR measurements, and the ability of the islets to reverse diabetes in nude mice.

However, the islets recovered by QMS without prior density gradient purification never exceeded 15% purity. This results in a situation of high recovery of labeled tissue accompanied by high contamination with unlabeled tissue, as recently reported in the literature on human islets.[17] It is hypothesized that uninfused tissue was being drafted by large agglomerations of free Dynabeads that accompany the digestate into the QMS. Such wide nets of linked magnetic Dynabeads can be clearly seen in Figure 4b. It is plausible that as these magnetic nets are drawn to the outer channel wall, unlabeled acinar tissue is caught up in the magnetic nets and contaminates the labeled islets. Possible methods for increasing the resulting purity of isolated labeled islets are (1) rinsing the infused lobe with buffer to remove most uninfused beads, (2) utilizing fewer or less magnetic beads, or (3) employing a weaker magnetic field so as to reduce the size of the nets of free Dynabeads within the suspension.

The QMS channel used in the current study was originally designed to purify rare cancer and stem cells. Noncritical dimensions within fittings and connections are appropriate for individual mammalian cells but not optimal for unpurified digested pancreatic tissue and islets. Preliminary estimates of the islet damage threshold limited throughput to a range that was not expected to damage microcarrier cultures[36] until the stress threshold for islets themselves is established. Ongoing studies in our laboratories will determine the maximum hydrodynamic forces that islets can sustain without damage so that optimum bioprocessing equipment can be designed.

Obtaining homogeneity of bead infusion and, more importantly, efficient magnetic purification of the labeled islets have proven difficult to achieve in the human[17] and porcine pancreas model. The difficulties in scaling-up are in part due to suboptimal bead infusion techniques, primarily because of incomplete understanding of the complex anatomy of the porcine pancreas vasculature and suboptimal flushing of the porcine pancreas before bead infusion. Consistent bead infusion and homogeneous distribution in porcine pancreata can be achieved through detailed understanding of the porcine pancreatic anatomy and modifications in the procurement and flushing techniques as well as the timing, location, mode of infusion, and the bead size, and concentration within the infused suspension. Effective magnetic purification of porcine (and human) islets will require the design of specific instrumentation tailored to the unique properties of islets.

In conclusion, proof of concept of preferential labeling of islets with magnetic beads and retrieving them after passing

them through QMS without compromising their viability and function has been demonstrated. However, difficulties in the use of the preclinical porcine model have been encountered, and solutions have been proposed. Should these solutions be successfully implemented, this technology can be ultimately applied to the routine and effective purification of porcine and human islets.

Acknowledgments

We thank and acknowledge the invaluable contribution of the members of our team who participated in this project: Jeffrey D. Ansite, Daniel W. Fraga, Hui-Jian Zhang, Baolin Liu, Muhamad H. Abdulla, Stathis Avgoustiniatos, Vinc Boyd, Thomas R. Gilmore, Lukas Guenther, Jian Q. Hao, Kristen Maynard, Kate Mueller, and Bill Scott.

Research funding was provided by grants from the National Institutes of Health (NIH), National Institute of Diabetes and Digestive and Kidney Diseases (R01DK068717), the Iacocca Foundation, the Schott Foundation, and the Carol Olson Memorial Diabetes Research Fund.

Disclosure Statement

No competing financial interests exist.

References

1. Fiorina, P., and Secchi, A. Pancreatic islet cell transplant for treatment of diabetes. Endocrinol Metab Clin N Am **36,** 999, 2007.
2. Hogan, A., Pileggi, A., and Ricordi, C. Transplantation: current developments and future directions; the future of clinical islet transplantation as a cure for diabetes. Front Biosci **13,** 1192, 2008.
3. Shapiro, A.M., Lakey, J.R., Ryan, E.A., Korbutt, G.S., Toth, E., Warnock, G.L., Kneteman, N.M., and Rajotte, R.V. Islet transplantation in seven patients with type 1 diabetes mellitus using a glucocorticoid-free immunosuppressive regimen. N Engl J Med **343,** 230, 2000.
4. Hering, B.J., Kandaswamy, R., Ansite, J.D., Eckman, P.M., Nakano, M., Sawada, T., Matsumoto, I., Ihm, S.H., Zhang, H.J., Parkey, J., Hunter, D.W., and Sutherland, D.E. Single-donor, marginal-dose islet transplantation in patients with type 1 diabetes. JAMA **293,** 830, 2005.
5. Frank, A., Deng, S., Huang, X., Velidedeoglu, E., Bae, Y.S., Liu, C., Abt, P., Stephenson, R., Mohiuddin, M., Thambipillai, T., Markmann, E., Palanjian, M., Sellers, M., Naji, A., Barker, C.F., and Markmann, J.F. Transplantation for type I diabetes: comparison of vascularized whole-organ pancreas with isolated pancreatic islets. Ann Surg **240,** 631, 2004.
6. Froud, T., Ricordi, C., Baidal, D.A., Hafiz, M.M., Ponte, G., Cure, P., Pileggi, A., Poggioli, R., Ichii, H., Khan, A., Ferreira, J.V., Pugliese, A., Esquenazi, V.V., Kenyon, N.S., and Alejandro, R. Islet transplantation in type 1 diabetes mellitus using cultured islets and steroid-free immunosupression: Miami experience. Am J Transplant **5,** 2037, 2005.
7. Badet, L., Benhamou, P.Y., Wojtusciszyn, A., Baertschiger, R., Milliat-Guittard, L., Kessler, L., Penfornis, A., Thivolet, C., Renard, E., Bosco, D., Morel, P., Morelon, E., Bayle, F., Colin, C., and Berney, T. Expectations and strategies regarding islet transplantation: metabolic data from the GRAGIL 2 trial. Transplantation **84,** 89, 2007.
8. Salvalaggio, P.R., Deng, S., Ariyan, C.E., Millet, I., Zawalich, W.S., Basadonna, G.P., and Rothstein, D.M. Islet filtration: a simple and rapid new purification procedure that avoids ficoll and improves islet mass and function. Transplantation **74,** 877, 2002.
9. Pinkse, G.G., Steenvoorde, E., Hogendoorn, S., Noteborn, M., Terpstra, O.T., Bruijn, J.A., and De Heer, E. Stable transplantation results of magnetically retracted islets: a novel method. Diabetologia **47,** 55, 2004.
10. Jahr, H., Pfeiffer, G., Hering, B.J., Federlin, K., and Bretzel, R.G. Endotoxin-mediated activation of cytokine production in human PBMCs by collagenase and ficoll. J Mol Med **77,** 118, 1999.
11. Scharp, D.W., Kemp, C.B., Knight, M.J., Ballinger, W.F., and Lacy, P.E. The use of ficoll in the preparation of viable islets of Langerhans from the rat pancreas. Transplantation **16,** 686, 1973.
12. Davies, J.E., James, R.F., London, N.J., and Robertson, G.S. Optimization of the magnetic field used for immunomagnetic islet purification. Transplantation **59,** 767, 1995.
13. Zborowski, M., Ostera, G.R., Moore, L.R., Milliron, S., Chalmers, J.J., and Schechter, A.N. Red blood cell magnetophoresis. Biophys J **84,** 2638, 2003.
14. Gauthier, V.J., and Mannik, M. A method for isolation of mouse glomeruli for quantitation of immune deposits. Kidney Int **33,** 897, 1988.
15. Baelde, H.J., Bergijk, E.C., and Bruijn, J.A. Isolation and characterization of mouse glomerular basement membrane. J Clin Lab Immunol **33,** 17, 1990.
16. Baelde, J.J., Bergijk, E.C., Hoedemaeker, P.J., de Heer, E., and Bruijn, J.A. Optimal method for RNA extraction from mouse glomeruli. Nephrol Dial Transplant **9,** 304, 1994.
17. Töns, H.A., Baranski, A.G., Terpstra, O.T., and Bouwman, E. Isolation of the islets of Langerhans from the human pancreas with magnetic retraction. Transplant Proc **40,** 413, 2008.
18. Sun, L., Zborowski, M., Moore, L.R., and Chalmers, J.J. Continuous, flow-through immunomagnetic cell sorting in a quadrupole field. Cytometry **33,** 469, 1998.
19. Tong, X., Xiong, Y., Zborowski, M., Farag, S.S., and Chalmers, J.J. A novel high throughput immunomagnetic cell sorting system for potential clinical scale depletion of T cells for allogeneic stem cell transplantation. Exp Hematol **35,** 1613, 2007.
20. Ricordi, C., Lacy, P.E., Finke, E.H., Olack, B.J., and Scharp, D.W. Automated method for isolation of human pancreatic islets. Diabetes **37,** 413, 1988.
21. Brandhorst, H., Brandhorst, D., Hering, B.J., and Bretzel, R.G. Significant progress in porcine islet mass isolation utilizing liberase HI for enzymatic low-temperature pancreas digestion. Transplantation **68,** 355, 1999.
22. Kirchhof, N., Shibata, S., Wijkstrom, M., Kulick, D.M., Salerno, C.T., Clemmings, S.M., Heremans, Y., Galili, U., Sutherland, D.E., Dalmasso, A.P., and Hering, B.J. Reversal of diabetes in non-immunosuppressed rhesus macaques by intraportal porcine islet xenografts precedes acute cellular rejection. Xenotransplantation **11,** 396, 2004.
23. McCloskey, K.E., Moore, L.R., Hoyos, M., Rodriguez, A., Chalmers, J.J., and Zborowski, M. Magnetophoretic cell sorting is a function of antibody binding capacity. Biotechnol Prog **19,** 899, 2003.
24. Jing, Y., Moore, L.R., Williams, P.S., Chalmers, J.J., Farag, S.S., Bolwell, B., and Zborowski, M. Blood progenitor cell separation from clinical leukapheresis product by magnetic

nanoparticle binding and magnetophoresis. Biotechnol Bioeng **96,** 1139, 2007.
25. Williams, P.S., Decker, K., Nakamura, M., Chalmers, J.J., Moore, L.R., and Zborowski, M. Splitter imperfections in annular split-flow thin separation channels: experimental study of nonspecific crossover. Anal Chem **75,** 6687, 2003.
26. Williams, P.S., Zborowski, M., and Chalmers, J.J. Flow rate optimization for the quadrupole magnetic cell sorter. Anal Chem **71,** 3799, 1999.
27. Hoyos, M., Moore, L.R., McCloskey, K.E., Margel, S., Zuberi, M., Chalmers, J.J., and Zborowski, M. Study of magnetic particles pulse-injected into an annular SPLITT-like channel inside a quadrupole magnetic field. J Chromatogr A **903,** 99, 2000.
28. Zhang, H., Moore, L.R., Zborowski, M., Williams, P.S., Margel, S., and Chalmers, J.J. Establishment and implications of a characterization method for magnetic nanoparticle using cell tracking velocimetry and magnetic susceptibility modified solutions. Analyst **130,** 514, 2005.
29. Zhang, H., Williams, P.S., Zborowski, M., and Chalmers, J.J. Binding affinities/avidities of antibody-antigen interactions: quantification and scale-up implications. Biotechnol Bioeng **95,** 812, 2006.
30. Papas, K.K., Pisania, A., Wu, H., Weir, G.C., and Colton, C.K. A stirred microchamber for oxygen consumption rate measurements with pancreatic islets. Biotechnol Bioeng **98,** 1071, 2007.
31. Avgoustiniatos, E.S., Dionne, K.E., Wilson, D.F., Yarmush, M.L., and Colton, C.K. Measurements of the effective diffusion coefficient of oxygen in pancreatic islets. Ind Eng Chem Res **46,** 6157, 2007.
32. Lara, O., Tong, X., Zborowski, M., Farag, S.S., and Chalmers, J.J. Comparison of two immunomagnetic separation technologies to deplete T cells from human blood samples. Biotechnol Bioeng **94,** 66, 2006.
33. Bonner-Weir, S., and Orci, L. New perspectives on the microvasculature of the islets of Langerhans in the rat. Diabetes **31,** 883, 1982.
34. Brunicardi, F.C., Stagner, J., Bonner-Weir, S., Wayland, H., Kleinman, R., Livingston, E., Guth, P., Menger, M., McCuskey, R., Intaglietta, M., Charles, A., Ashley, S., Cheung, A., Ipp, E., Gilman, S., Howard, T., and Passaro, E., Jr. Microcirculation of the islets of Langerhans. Diabetes **45,** 385, 1996.
35. Ferrer-Fabrega, J., Scott III, W.E., Matsumoto, S., Suszynski, T., Weegman, B., Sutherland, D.E.R., Hering, B.J., and Papas, K.K. Porcine pancreas anatomy: implications in pancreas procurement, preservation and islet Isolation. Transplantation **86,** 1503, 2008.
36. Gregoriades, N., Clay, J., Ma, N., Koelling, K., and Chalmers, J.J. Cell damage of microcarrier cultures as a function of local energy dissipation created by a rapid extensional flow. Biotechnol Bioeng **69,** 171, 2000.

Address reprint requests to:
Klearchos K. Papas, Ph.D.
Diabetes Institute for Immunology and Transplantation
University of Minnesota Medical School
Mayo Mail Code 280
420 Delaware St.
SE Minneapolis, MN 55455

E-mail: papas006@umn.edu.

Received: June 19, 2008
Accepted: July 7, 2008
Online Publication Date: May 29, 2009